Space Filling Curves for MRI Sampling

Sharma, Shubham; Hari, K.V.S.; Leus, Geert

DOI
10.1109/ICASSP40776.2020.9054372

Publication date
2020

Document Version
Final published version

Published in
ICASSP 2020 - 2020 IEEE International Conference on Acoustics, Speech and Signal Processing (ICASSP)

SPACE FILLING CURVES FOR MRI SAMPLING

Shubham Sharma, K.V.S. Hari

Electrical Communication Engineering Dept.
Indian Institute of Science
Bengaluru, India

Geert Leus

Circuits and Systems
Dept. of Microelectronics, EEMCS
Delft University of Technology
Delft, Netherlands

ABSTRACT

A novel class of k-space trajectories for magnetic resonance imaging (MRI) sampling using space filling curves (SFCs) is presented here. More specifically, Peano, Hilbert and Sierpinski curves are used. We propose 1-shot and 4-shot variable density SFCs by utilizing the space coverage provided by SFCs in different iterations. The proposed trajectories are compared with state-of-the-art echo planar imaging (EPI) trajectories for 128×128 and 256×256 phantom and brain images. The simulation results show that the readout time is reduced by up to 45% for the 128×128 image with little compromise in reconstruction quality. Also, the peak signal-to-noise ratio (PSNR) and structural similarity (SSIM) index are improved by 2.32 dB and 0.1009, respectively, with an 18% shorter readout time using the 4-shot Hilbert SFC trajectory for reconstructing a 256×256 brain MRI image.

***Index Terms*—** MRI, k-space trajectories, space filling curves

1. INTRODUCTION

Magnetic resonance imaging (MRI) is an important yet time consuming medical imaging method. The scan time in MRI is limited due to physical constraints of the system such as gradient limitations, sampling rate constraints and a low signal-to-noise ratio (SNR). Over the last decades many methods have been proposed to reduce the scan time to facilitate comfort for the patients and to overcome these physical limitations. Methods such as parallel imaging [1–3], rapid acquisition with relaxation enhancement (RARE) [4], fast low-angle shot (FLASH) [5], fast imaging with steady state precession (FISP) [6] and echo planar imaging (EPI) [7] have been extensively studied and used to reduce the scan time. Recent developments in compressed sensing (CS) theory [8, 9] also allow the scan time to be reduced considerably [10, 11]. The data can now be sampled sparsely and the image can be obtained using non-linear reconstruction methods [12].

From the physics of the system, the signal received can be directly mapped to the frequency space (2D/3D), known as the k-space in the MRI community. The path along which the data is collected in the k-space is called a k-space trajectory and it is governed by the magnetic gradients $\mathbf{g}_i(t)$, $i = \{x, y, z\}$ as $\mathbf{k}_i(t) = \gamma \int_0^t \mathbf{g}_i(\tau) d\tau$, where γ is the gyromagnetic ratio (42.58MHz/T for Hydrogen). The most common trajectories are Cartesian, spiral [13, 14] and radial [15]. EPI [16] is a Cartesian-based fast scanning method that samples the complete k-space in a single shot. However, it suffers from drawbacks like poor image reconstruction quality and loud acoustic noise which makes the patients uncomfortable. In recent years, non-Cartesian trajectories have received a lot of attention as they provide incoherent artifacts with undersampling and are more robust to motion [17–19]. The time taken to traverse the k-space depends on the length of the trajectory. The design of optimal k-space trajectories is still an open problem in the MRI community, yet some improvements have been made based on the theory of CS. In this work, we use space filling curves (SFCs) [20] as trajectories to sample the k-space and use the CS framework for reconstructing the image. SFCs have been used previously for designing trajectories for MRI as a method to reduce the acoustic noise [21]. In that paper, the authors use a Hilbert-Moore SFC (a modified Hilbert SFC) trajectory which is observed to be robust to eddy currents. We explore SFC-based trajectories further to reduce the readout time.

2. SPACE FILLING CURVES

An SFC provides a continuous mapping from a compact interval I to a multidimensional space $\mathbb{R}^n$ such that the curve passes through every point in the space $\mathbb{R}^n$ exactly once. These curves are constructed iteratively as a sequence of continuous piecewise linear curves. Depending on the shape of the curve, SFCs can be of different kinds, e.g., Peano, Hilbert, Sierpinski, Dragon, Gosper and others. The Hilbert curve is the most commonly used in a variety of applications. Figure 1 shows Peano, Hilbert and Sierpinski SFCs up to 3 iterations. To construct these figures, we consider 2D space and use a recursive method for generating the SFCs.

2.1. Variable density SFCs for k-space sampling

Variable density (VD) sampling is an integral part of designing k-space trajectories. This is because the center of the k-space contains more energy than the boundary region. Another theory supporting VD sampling of k-space comes from the varying sparsity depending on the scale of the wavelet basis under a CS framework. To take care of this, we propose

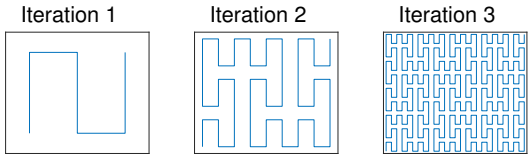

(a) Peano SFC.

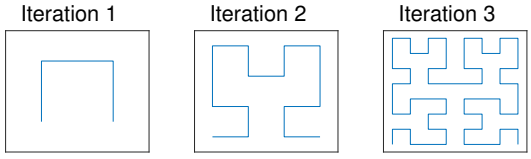

(b) Hilbert SFC.

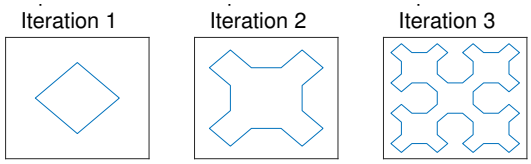

(c) Sierpinski SFC.

Fig. 1: Various space filling curves up to three iterations.

variable density SFCs that sample the region near the center of the k-space with an SFC at an iteration higher than the SFC near the boundary region. This results in more points at the center region of the k-space compared to the boundary region.

VD SFCs are constructed by first dividing the k-space into multiple sections as shown in Fig. 2(a). The section at the center of the k-space is traversed using an SFC with I_c iterations. This section extends from $-k_{\max}/2$ to $+k_{\max}/2$ along both axes. The boundary of the k-space is divided into 12 smaller sections. Each section is traversed using an SFC with I_b, where $I_b < I_c$. Figure 3 shows examples of VD Peano, Hilbert and Sierpinki SFCs. In each case, the SFC with I_b iterations is taken as reference and is rotated and/or flipped such that the ending point of the SFC in one section is nearest to the starting point of the next section. The transformations related to the various SFCs are different from others as the starting and ending points vary according to the SFC considered. For example, in the Peano curve, the starting and ending points are diagonal to each other. In case of the Hilbert curve, they are at adjacent corners of the space. In the Sierpinski curve, the starting and ending points are the same and hence, there is a line across one section to reach the next section. Further, fine sampling of the center of the k-space is also done for a better image reconstruction in all cases.

2.2. Multi-shot VD SFCs for *k*-space sampling

In MRI, the intensity of the received signal reduces with time during each excitation. Hence, for the reconstruction of images of higher resolution (256×256 or 512×512), the k-space is traversed using multiple RF excitations and the trajectory is known as a multi-shot trajectory. To construct multi-shot SFC trajectories, the k-space is divided into four quadrants as shown in Fig. 2(b). Each quadrant is to be traversed separately using a VD SFC trajectory. To do this, each quadrant is further divided into four sections. The section near the center of the k-space is traversed with an SFC of I_c iterations. The remaining three sections are traversed using an SFC with I_b iterations ($I_b < I_c$). Similar to the VD SFC described in the previous section, the reference SFC of I_b iterations is rotated and/or flipped to obtain continuity while moving from one section to the next. Figure 4 shows examples of 4-shot VD SFCs based on Peano, Hilbert and Sierpinski curves. As before, the center of the k-space is again fine sampled.

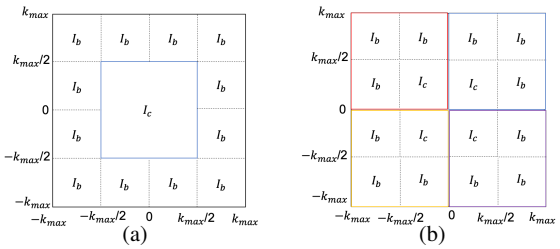

(a) (b)

Fig. 2: Construction of (a) single-shot VD SFC trajectories; (b) 4-shot VD SFC trajectories.

2.3. EPI trajectory

An EPI trajectory scans the complete k-space uniformly in a single RF excitation (single-shot). EPI covers the k-space line-by-line using small blips in the gradient to move to the next line. For high resolution images, a larger k-space is sampled using a multi-shot EPI trajectory. This uses multiple RF excitations to traverse the k-space in parts.

2.4. Feasible trajectory

The hardware and the safety concern in an MRI machine restrict the amount of current through the gradient coils resulting in gradient constraints of maximum amplitude ($G_{\max}$) and slew rate ($S_{\max}$). As a result, the traversal of the k-space trajectories will be limited in velocity ($v_{\max} = \gamma G_{\max}$) and acceleration ($a_{\max} = \gamma S_{\max}$). The SFC and EPI trajectories are defined by a few control points and are infeasible. The actual points to be sampled along these trajectories such that they satisfy the aforementioned constraints are obtained by the optimal control-based method proposed in [22], known as the time-optimal control (TOC) method. This method provides the fastest gradients to traverse a given trajectory with given start and end points and hence it results in a variable velocity. For this method, the trajectory near the sharper edges will be traversed more slowly than along the smoother parts. This happens because near the sharp edges the slew rate constraint is not satisfied and the trajectory needs to be traversed slower. This means there are more sample points near the sharp edges than along the smoother parts.

3. NUMERICAL EXPERIMENTS

3.1. Reconstruction using compressed sensing

MR images are sparse in the wavelet, finite differences and DCT domains. By the physics of the system, the sampling is

Trajectory	I_c	I_b	Time (ms)	SSIM	PSNR
Peano	2	1	50.34	0.8419	25.41 dB
Peano	3	1	**84.44**	**0.9858**	**35.72 dB**
Peano	3	2	139.86	0.9996	53.21 dB
Hilbert	3	2	63.99	0.9204	31.59 dB
Hilbert	4	2	**80.41**	**0.9829**	**38.75 dB**
Hilbert	4	3	130.55	0.9991	49.90 dB
Hilbert	5	2	127.03	0.9984	43.81 dB
Sier.	3	1	62.15	0.9465	32.22 dB
Sier.	3	2	**77.19**	**0.9820**	**38.22 dB**
Sier.	4	1	97.62	0.9938	38.53 dB
Sier.	4	2	112.67	0.9983	46.08 dB
EPI	-	-	141.86	0.9926	52.07 dB

Table 1: Reconstruction performance for the 128×128 Shepp-Logan phantom image.

in the frequency domain (k-space). Under this setup, the use of CS techniques was proposed in [10] such that an undersampled k-space can be used to reconstruct a 2D image $\mathbf{X}$ as follows:

$$\hat{\mathbf{X}} = \arg\min_{\mathbf{X}} ||\mathrm{NFFT}(\mathbf{X}) - \mathbf{Y}||_2^2 + \lambda_1 ||\mathcal{W}(\mathbf{X})||_1 + \lambda_2 ||\mathbf{X}||_{\mathrm{TV}}$$

where $\mathbf{Y}$ is the observed k-space data, NFFT is the nonuniform fast Fourier transform, $\mathcal{W}(\cdot)$ is the wavelet transform and $||\cdot||_{\mathrm{TV}}$ is the total variation (TV) norm. This problem is solved using non-linear conjugate gradient with a fast and cheap backtracking line-search [10, 23].

3.2. Simulation setup

We compare the image reconstruction quality by two measures: structural similarity (SSIM) index and peak signal-to-noise ratio (PSNR). SSIM provides a comparison in perception of the two images and PSNR is a measure of the error in intensity values. The performances of single-shot EPI and VD SFC trajectories are compared for reconstructing the 128×128 Shepp-Logan phantom using different iterations. The performances of 4-shot SFC trajectories are compared for two 256×256 images: a realistic brain phantom [24] and a T1-weighted sagittal brain MRI image as shown in Fig. 4(a). To obtain the feasible trajectories, the gradient constraints used are $G_{\max} = 40$mT/m and $S_{\max} = 150$mT/m/ms which is standard for 3T MRI machines. The sampling duration is taken as $t_s = 0.004$ ms. The k-space data along different trajectories is calculated by taking the inverse Fourier transform of the image. The image is then reconstructed using the CS method described above. All simulations have been performed in MATLAB 2017b. In a practical scenario, the gradients start and end from zero. Hence, all the trajectories used for simulations are designed to start and end at the center of the k-space.

3.3. Simulation results and discussion

We compare the readout times and reconstruction performance for single-shot VD SFCs of different I_cs and I_bs for the 128×128 Shepp-Logan phantom image in Table 1. The center of the k-space is sampled densely in each case. With increasing iterations, the readout time increases, resulting in better reconstruction performance. These are also compared

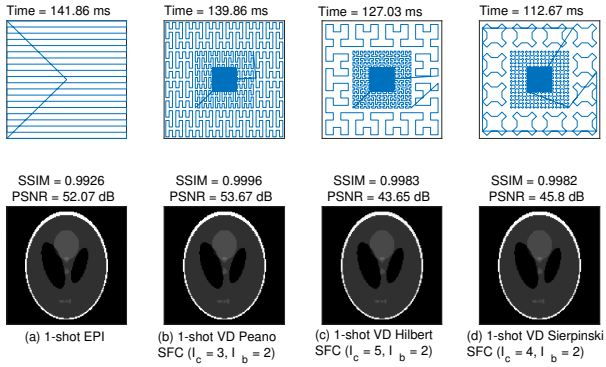

Fig. 3: Performance comparison of 1-shot VD SFC trajectories with EPI for reconstructing the 128×128 Shepp-Logan phantom image.

Traj.	I_c	I_b	Time (ms)	SSIM	PSNR	SSIM	PSNR
Peano	3	1	34.19	0.5119	22.29 dB	0.6160	24.74 dB
Peano	3	2	48.10	0.5163	22.77 dB	0.6214	24.65 dB
Peano	4	1	159.03	0.9788	33.68 dB	0.9534	34.57 dB
Hilbert	6	3	**58.12**	**0.7500**	**29.43 dB**	**0.7678**	**29.01 dB**
Hilbert	6	4	70.59	0.7830	31.17 dB	0.7871	29.70 dB
Hilbert	6	5	105.32	0.7821	31.32 dB	0.7842	29.64 dB
Sier.	5	3	**55.46**	0.5797	23.67 dB	**0.7158**	**27.39 dB**
Sier.	5	4	81.87	0.6043	23.99 dB	0.7110	27.47 dB
Sier.	6	1	113.53	0.9763	33.26 dB	0.9517	34.43 dB
EPI	-	-	71.66	0.6548	28.26 dB	0.6669	26.69 dB

Table 2: Reconstruction performance for the 256×256 realistic brain phantom and MRI images.

with the single-shot EPI trajectory which provides an SSIM and PSNR of 0.9926 and 52.07 dB with a readout time of 141 ms. A similar performance is observed using different SFCs, for example, the VD Peano trajectory ($I_c = 3$, $I_b = 2$) gives the same performance for the same readout time. The Hilbert ($I_c = 5$, $I_b = 2$) and the Sierpinski ($I_c = 4$, $I_b = 2$) trajectories also provide similar reconstruction performance yet with shorter readout times. These trajectories and reconstructed images are shown in Fig. 3. Note that the EPI trajectory shown in the figure is displayed with less lines for clarity. The EPI trajectory used actually samples 128 lines in the k-space. Also, using the Peano ($I_c = 3$, $I_b = 1$), the Hilbert ($I_c = 4$, $I_b = 2$) and the Sierpinski ($I_c = 3$, $I_b = 2$) trajectories, with little compromise in the reconstruction performance in terms of SSIM, readout time is significantly reduced.

For the 256×256 images, 4-shot versions of the EPI and SFC trajectories are compared in Table 2. The readout times shown in the table are per shot. The EPI trajectory takes 71 ms per shot to provide an SSIM of 0.6548 and a PSNR of 28.26 dB for the realistic brain phantom image. For the brain MRI image it provides an SSIM and PSNR of 0.6669 and 26.69 dB, respectively. The 4-shot VD SFC trajectories are created with different I_cs and I_bs. Similar to the previous case, with increasing iterations in SFC the readout time increases with an improvement in reconstruction performance.

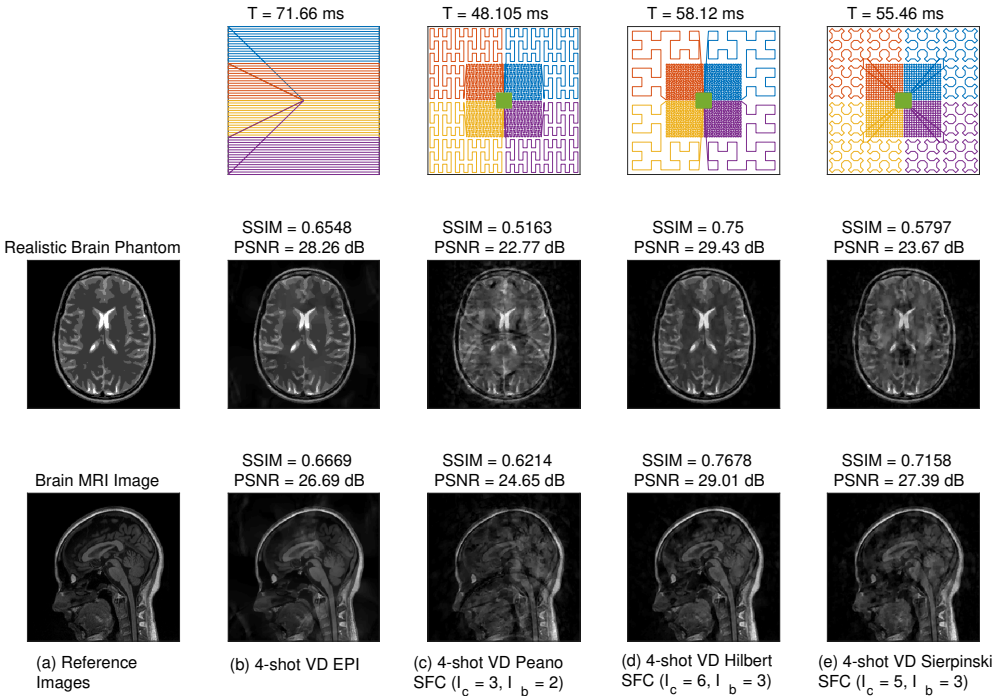

Fig. 4: Performance comparison of 4-shot (b) EPI, (c) VD Peano SFC, (d) VD Hilbert SFC, (e) VD Sierpinsky SFC trajectories for reconstructing the 256×256 analytical brain phantom image and a brain MRI image.

The Peano trajectory does not result in a readout time close to what is achieved with EPI due to its design. Using the 4-shot VD Hilbert trajectory ($I_c = 6$, $I_b = 4$), for a similar readout time, the reconstruction performance is improved significantly for both images. It also provides improved performance for $I_c = 6$, $I_b = 3$ with a reduction in readout time at the same time. The 4-shot Sierpinski trajectory improves the reconstruction performance for the brain MRI image for a shorter readout time of 55 ms (reduction by 22%) for $I_c = 5$, $I_b = 3$. These trajectories and their reconstructed images are shown in Fig. 4.

We study the density of points, i.e, the number of points per unit square area on the k-space. The density of points in an area will depend on the iteration number of the SFC used to construct the trajectory since an SFC with more iterations is more dense. In general, as one moves from the center to the boundary, the density of points decreases. A normalized density plot for the three SFC trajectories shown in Fig. 4 is given in Fig. 5. The k-space is divided in 20 square units and the number of sample points in each are found for each trajectory. The 9^{th} row (center) is plotted in the figure. Due to dense sampling near the center, we see more points in the middle of the curves.

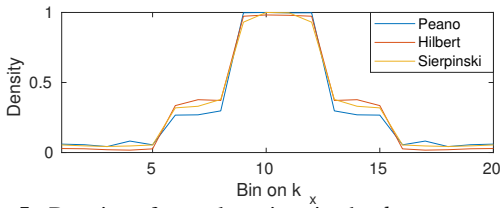

Fig. 5: Density of sample points in the k-space covered by 4-shot VD Peano, Hilbert and Sierpinski trajectories.

4. CONCLUSION

The performance of different SFCs as k-space trajectories for sampling in MRI under a CS scheme has been investigated here. Variable density muti-shot SFCs have been proposed to reconstruct high resolution MRI images. SFCs with different iterations provide trajectories with different readout time and reconstruction performance. The performance of the proposed trajectories is compared with the state-of-the-art EPI trajectory. Compared to the EPI trajectory, VD Hilbert SFCs are able to improve the reconstruction performance with about 19% shorter readout time. For applications such as dynamic cardiac imaging and real-time speech MRI, the proposed Hilbert SFCs will be useful.

5. ACKNOWLEDGEMENT

The authors would like to thank Prof. Navin Kashyap for his inputs and support. We would also like to thank the Ministry of Electronics and Information Technology (MeitY), India for the financial support. We are also grateful to the IISc-TU Delft collaboration agreement.

6. REFERENCES

[1] Daniel K Sodickson and Warren J Manning, "Simultaneous acquisition of spatial harmonics (SMASH): fast imaging with radiofrequency coil arrays," *Magnetic Resonance in Medicine*, vol. 38, no. 4, pp. 591–603, 1997.

[2] Klaas P Pruessmann, Markus Weiger, Markus B Scheidegger, Peter Boesiger, et al., "SENSE: sensitivity encoding for fast MRI," *Magnetic Resonance in Medicine*, vol. 42, no. 5, pp. 952–962, 1999.

[3] Mark A Griswold, Peter M Jakob, Robin M Heidemann, Mathias Nittka, Vladimir Jellus, Jianmin Wang, Berthold Kiefer, and Axel Haase, "Generalized autocalibrating partially parallel acquisitions (GRAPPA)," *Magnetic Resonance in Medicine*, vol. 47, no. 6, pp. 1202–1210, 2002.

[4] J Hennig, A Nauerth, and H Friedburg, "RARE imaging: a fast imaging method for clinical MR," *Magnetic Resonance in Medicine*, vol. 3, no. 6, pp. 823–833, 1986.

[5] Jens Frahm, Axel Haase, and Dieter Matthaei, "Rapid three-dimensional MR imaging using the FLASH technique.," *Journal of Computer Assisted Tomography*, vol. 10, no. 2, pp. 363–368, 1986.

[6] GH Glover and NJ Pelc, "A rapid-gated cine MRI technique," in *Magnetic Resonance Annual.* 1988.

[7] P Mansfield, "Multi-planar image formation using NMR spin echoes," *Journal of Physics: Solid State Physics*, vol. 10, no. 3, pp. L55, 1977.

[8] Emmanuel J Candès et al., "Compressive sampling," in *Proceedings of the International Congress of Mathematicians*. Madrid, Spain, 2006, vol. 3, pp. 1433–1452.

[9] David L Donoho, "Compressed sensing," *IEEE Transactions on Information Theory*, vol. 52, no. 4, pp. 1289–1306, 2006.

[10] Michael Lustig, David Donoho, and John M Pauly, "Sparse MRI: The application of compressed sensing for rapid MR imaging," *Magnetic Resonance in Medicine*, vol. 58, no. 6, pp. 1182–1195, 2007.

[11] Michael Lustig, David L Donoho, Juan M Santos, and John M Pauly, "Compressed sensing MRI," *IEEE Signal Processing Magazine*, vol. 25, no. 2, pp. 72–82, 2008.

[12] Shiqian Ma, Wotao Yin, Yin Zhang, and Amit Chakraborty, "An efficient algorithm for compressed MR imaging using total variation and wavelets," in *IEEE Conference on Computer Vision and Pattern Recognition (CVPR)*. IEEE, 2008, pp. 1–8.

[13] Richard S Likes, "Moving gradient zeugmatography," Dec. 22 1981, US Patent 4,307,343.

[14] Dong-hyun Kim, Elfar Adalsteinsson, and Daniel M Spielman, "Simple analytic variable density spiral design," *Magnetic Resonance in Medicine*, vol. 50, no. 1, pp. 214–219, 2003.

[15] PC Lauterbur, "Image formation by induced local interactions: examples employing nuclear magnetic resonance," 1973.

[16] M. A. Bernstein, K. F. King, and X. J. Zhou, *Handbook of MRI Pulse Sequences*, Elsevier Academic Press, 2004.

[17] Nicolas Chauffert, Philippe Ciuciu, Pierre Weiss, and Fabrice Gamboa, "From variable density sampling to continuous sampling using Markov chains," *Proceedings of the 10th SampTA Conference*, pp. 200–203, 2013.

[18] Nicolas Chauffert, Philippe Ciuciu, Jonas Kahn, and Pierre Weiss, "Travelling salesman-based variable density sampling," *Proceedings of the 10th SampTA Conference*, pp. 509–512, 2013.

[19] Carole Lazarus, Pierre Weiss, Nicolas Chauffert, Franck Mauconduit, Loubna El Gueddari, Christophe Destrieux, Ilyess Zemmoura, Alexandre Vignaud, and Philippe Ciuciu, "SPARKLING: variable-density k-space filling curves for accelerated T2*-weighted MRI," *Magnetic resonance in medicine*, vol. 81, no. 6, pp. 3643–3661, 2019.

[20] H. Sagan, *Space-Filling Curves*, Springer Verlag, 1994.

[21] Wolf Daniel Blecher, *The Hilbert-Moore sequence Acoustic Noise optimized MR Imaging*, Ph.D. thesis, Universität Mannheim, 2008.

[22] Michael Lustig, Seung-Jean Kim, and John M Pauly, "A fast method for designing time-optimal gradient waveforms for arbitrary k-space trajectories," *IEEE Transactions on Medical Imaging*, vol. 27, no. 6, pp. 866–873, 2008.

[23] M Lustig, "SparseMRI toolbox downloaded from http://www.eecs.berkeley.edu/m̃lustig/software.html," 2014.

[24] Matthieu Guerquin-Kern, L Lejeune, Klaas Paul Pruessmann, and Michael Unser, "Realistic analytical phantoms for parallel magnetic resonance imaging," *IEEE Transactions on Medical Imaging*, vol. 31, no. 3, pp. 626–636, 2012.